INTERNATIONAL JOURNAL OF
NUMERICAL ANALYSIS AND MODELING
Volume 1, Number 1, Pages 1–18

CHEBYSHEV SPECTRAL METHOD FOR UNSTEADY AXISYMMETRIC MIXED CONVECTION HEAT TRANSFER OF POWER LAW FLUID OVER A CYLINDER WITH VARIABLE TRANSPORT PROPERTIES

JIAJIA NIU, LIANCUN ZHENG, YANG YANG, AND CHI-WANG SHU

Abstract. In this work, we study the unsteady axisymmetric mixed convection boundary layer flow and heat transfer of non-Newtonian power law fluid over a cylinder. Different from most classical works, the temperature dependent variable fluid viscosity and thermal conductivity are taken into account in highly coupled velocity and temperature fields. The motion of the fluid can be modeled by a time-dependent nonlinear parabolic system in cylindrical coordinates, which is solved numerically by using Chebyshev spectral method along with the strong stability preserving (SSP) third order Runge-Kutta time discretization. We apply the numerical solver to problems with different power law indices, viscosity parameter, thermal conductivity parameter and Richardson numbers, and compute up to the steady state. The numerical solver is checked by testing the spectral convergence of the numerical approximation to a smooth exact solution of the PDEs with source terms. Moreover, the combined effects of pertinent physical parameters on the flow and heat transfer characteristics are analyzed in detail.

Key Words. Unsteady mixed convection, power law fluid, temperature dependent fluid viscosity, variable thermal conductivity, Chebyshev spectral method.

1. Introduction

Mixed convection (combined forced and free convection) flows are of interest and importance in a wide variety of fields such as petroleum, nuclear and environmental engineering. Flow over a slender cylinder is generally considered as axisymmetric instead of three dimensional problems, and the transverse curvature term contained in the governing equations strongly influences the velocity and temperature fields. Thus it has attracted great attention in the fields of steady/unsteady mixed convection flows under different situations [4, 13, 2, 12, 24].

One of the classical models of mixed convection flow is based on Newtonian fluid, which has been studied intensively. For steady flows, Kumari et al. [10] analyzed the effects of localized cooling/heating and suction/injection with a finite discontinuity on the mixed convection boundary layer flow in a thin vertical cylinder. Later, Mukhopadhyay [14] considered the axisymmetric mixed convection flow towards a stretching cylinder embedded in porous medium. Subsequently, Kaya [9] extended the problem to the case when the porosity of the porous medium is high,

2000 *Mathematics Subject Classification.* 35K55, 76A05, 76M22, 80A20.

The work of the first and second authors is supported by the National Natural Science Foundations of China (No. 51076012, NO. 51276014). The work of the last author is supported by ARO grant W911NF-11-1-0091 and NSF grant DMS-1112700.

and non-similar solutions were obtained by the Keller-box method. For unsteady flows, unsteady mixed convection flow over a rotating vertical slender cylinder has been studied in [21]. Recently, Patil et al. [16] obtained a non-similar solution of an unsteady mixed convection boundary layer flow over a non-linearly stretching vertical slender cylinder, where the slender cylinder velocity varies arbitrarily with time.

Besides the above, there are also some works on nanofluids. Grosan et al. [6] investigated the axisymmetric mixed convection flow past a thin vertical cylinder placed in a water-based copper (Cu) nanofluid. Moreover, Rashad et al. [20] studied the mixed convection boundary layer flow over a horizontal cylinder filled with a nanofluid, where they incorporated the Brownian motion and thermophoresis.

Another model is based on non-Newtonian fluid, which is a very commonly used model for gelled propellant fluid in aerospace application, foam fluid in petroleum industry, blood fluid in hemodynamic et al. [26, 25, 15]. However, there are only a few papers in the literature that deal with mixed convection flow of non-Newtonian fluid, and most works are on the inflow in the radial direction. For example, mixed convection from a heated semi-circular cylinder to power-law fluids in the steady flow regime is studied in [3, 1], and the unsteady flow was considered by Patnana et al. [17].

In all the above mentioned works, the thermo-physical properties of the fluid were assumed to be constant. However, these physical properties, especially fluid viscosity and thermal conductivity are affected by temperature [7, 11, 18, 19, 22, 23]. To the best of the authors' knowledge, little research was conducted for considering variable thermo-physical properties to boundary layer flows over a slender cylinder, especially the studies on unsteady flow of non-Newtonian fluid. In this paper, we focus on the effects of variable transport properties on unsteady mixed convection heat transfer of power law fluid.

Motivated by the above mentioned works, we perform our work in three aspects. First, we study the unsteady axisymmetric flow of a non-Newtonian power law fluid past a slender cylinder. Second, we consider the temperature dependent fluid properties. Third, we focus on developing numerical solutions with high-accuracy obtained by the Chebyshev spectral method [8], which can be sped up by the technique of Fast Fourier Transform (FFT).

2. Mathematical formulation

In this section, we construct the parabolic system to be solved numerically. Consider the unsteady axisymmetric mixed convection boundary layer flow over a vertical permeable slender cylinder of radius R placed in a non-Newtonian power law fluid with power law index n. Let t be the time variable and (u, v) be the velocity field along the (x, r) directions, where x and r are the axial and radial coordinates, respectively. By using the cylindrical coordinates, the domain is $(x, r) \in [0, +\infty) \times [R, +\infty)$. The density, velocity and temperature of the free flow at a remote distance from the cylinder are given by ρ_∞, U_∞ and T_∞, while the temperature of the static cylinder is T_W. The volumetric coefficient of thermal expansion is given as β_0, and the specific heat at constant temperature is assumed to be C_p. Under these assumptions, the governing equations for the mixed convection boundary layer equations are written as:

$$\frac{\partial u}{\partial x} + \frac{\partial v}{\partial r} + \frac{v}{r} = 0, \tag{1}$$

(2)
$$\rho_\infty\left(\frac{\partial u}{\partial t}+u\frac{\partial u}{\partial x}+v\frac{\partial u}{\partial r}\right)=\frac{1}{r}\frac{\partial}{\partial r}\left\{r\frac{\mu_\infty}{\left[1+\gamma^*\left(T-T_\infty\right)\right]}\left|\frac{\partial u}{\partial r}\right|^{n-1}\frac{\partial u}{\partial r}\right\}+\rho_\infty g\beta_0\left(T-T_\infty\right),$$

$$(3)\quad \left(\rho_\infty C_P\right)\left(\frac{\partial T}{\partial t}+u\frac{\partial T}{\partial x}+v\frac{\partial T}{\partial r}\right)=\frac{1}{r}\frac{\partial}{\partial r}\left\{k_\infty\left(1+\varepsilon\frac{T-T_\infty}{T_W-T_\infty}\right)r\frac{\partial T}{\partial r}\right\},$$

with the initial and boundary conditions given as follows.
Non-slip condition:

$$(4)\qquad u\left(x,R,t\right)=0,\quad v\left(x,R,t\right)=0,\quad T\left(x,R,t\right)=T_W,$$

matching with outer flow:

$$(5)\qquad \lim_{r\to+\infty}u\left(x,r,t\right)=U_\infty,\quad \lim_{r\to+\infty}T\left(x,r,t\right)=T_\infty,$$

inlet condition:

$$(6)\qquad u\left(0,r,t\right)=U_\infty,\quad T\left(0,r,t\right)=T_\infty,$$

initial condition:

$$(7)\qquad u\left(x,r,0\right)=u_0,\quad T\left(x,r,0\right)=T_0.$$

Here we consider the semi-empirical formula for the variable dynamic viscosity and thermal conductivity of the form [18, 19]:

$$(8)\qquad \frac{1}{\mu\left(T\right)}=\frac{1}{\mu_\infty}\left[1+\gamma^*\left(T-T_\infty\right)\right],\quad k\left(T\right)=k_\infty\left(1+\varepsilon\frac{T-T_\infty}{T_W-T_\infty}\right),$$

where γ^* is the thermal property of the fluid, ε is the thermal conductivity parameter, and μ_∞, k_∞ are the dynamic viscosity and thermal conductivity of the fluid far away from the cylinder, respectively.

Upon making use of the following dimensionless variables:

$$(9)\quad \bar{t}=\frac{Au_\infty}{R}t,\bar{x}=\frac{Ax}{R},\bar{r}=\frac{r}{R},\bar{u}=\frac{u}{u_\infty},\bar{v}=\frac{v}{Au_\infty},\bar{T}=\frac{T-T_\infty}{T_w-T_\infty},A=\frac{u_\infty^{n-2}\mu_\infty}{R^n\rho_\infty},$$

the dimensionless governing equations can be written as:

$$(10)\qquad \frac{\partial\bar{u}}{\partial\bar{x}}+\frac{\partial\bar{v}}{\partial\bar{r}}+\frac{\bar{v}}{\bar{r}}=0,$$

$$(11)\qquad \frac{\partial\bar{u}}{\partial\bar{t}}+\bar{u}\frac{\partial\bar{u}}{\partial\bar{x}}+\bar{v}\frac{\partial\bar{u}}{\partial\bar{r}}=\frac{1}{\bar{r}}\frac{\partial}{\partial\bar{r}}\left(\left(\frac{\theta_r}{\theta_r-\bar{T}}\right)\bar{r}\left|\frac{\partial\bar{u}}{\partial\bar{r}}\right|^{n-1}\frac{\partial\bar{u}}{\partial\bar{r}}\right)+Ri\bar{T},$$

$$(12)\qquad \frac{\partial\bar{T}}{\partial\bar{t}}+\bar{u}\frac{\partial\bar{T}}{\partial\bar{x}}+\bar{v}\frac{\partial\bar{T}}{\partial\bar{r}}=\frac{1}{\mathrm{Pr}}\frac{1}{\bar{r}}\frac{\partial}{\partial\bar{r}}\left(\left(1+\varepsilon\bar{T}\right)\bar{r}\frac{\partial\bar{T}}{\partial\bar{r}}\right),$$

with the corresponding dimensionless initial and boundary conditions:

$$(13)\qquad \bar{u}\left(\bar{x},1,\bar{t}\right)=0,\quad \bar{v}\left(\bar{x},1,\bar{t}\right)=0,\quad \bar{T}\left(\bar{x},1,\bar{t}\right)=1,$$

$$(14)\qquad \lim_{\bar{r}\to+\infty}\bar{u}\left(\bar{x},\bar{r},\bar{t}\right)=1,\quad \lim_{\bar{r}\to+\infty}\bar{T}\left(\bar{x},\bar{r},\bar{t}\right)=0,$$

$$(15)\qquad \bar{u}\left(-1,\bar{r},\bar{t}\right)=1,\quad \bar{T}\left(-1,\bar{r},\bar{t}\right)=0,$$

$$(16)\qquad \bar{u}\left(\bar{x},\bar{r},0\right)=\bar{u}_0,\quad \bar{T}\left(\bar{x},\bar{r},0\right)=\bar{T}_0.$$

The corresponding dimensionless groups that appeared in the governing equations are defined as:

$$Ri = \frac{g\beta_\infty (T_w - T_\infty)R}{u_\infty^2 A}, \quad \mathrm{Pr} = \frac{C_p \mu_\infty u_\infty^{n-1}}{k_\infty R^{n-1}}, \quad \theta_r = -\frac{1}{\gamma^* (T_W - T_\infty)}, \tag{17}$$

where Ri is the Richardson number, Pr is the Prandtl number, θ_r is the variable viscosity parameter with $\theta_r < 0$ for fluid and $\theta_r > 1$ for gas. In this paper, we consider $\theta_r < 0$ only.

We present:

$$\xi = 1 - 2e^{-\bar{x}}, \quad \eta = 1 - 2e^{-\bar{r}+1}, \tag{18}$$

which is the mapping from the semi-infinite domain $\bar{x} \in [0, +\infty), \bar{r} \in [1, +\infty)$ to a bounded one $\xi \in [-1, 1], \eta \in [-1, 1]$, and then we have:

$$\frac{\partial \bar{u}}{\partial \xi}(1-\xi) + \frac{\partial \bar{v}}{\partial \eta}(1-\eta) + \frac{\bar{v}}{1 - \ln\left(\frac{1-\eta}{2}\right)} = 0, \tag{19}$$

$$\begin{aligned} \tfrac{\partial \bar{u}}{\partial \bar{t}} + \bar{u}\tfrac{\partial \bar{u}}{\partial \xi}(1-\xi) + \bar{v}\tfrac{\partial \bar{u}}{\partial \eta}(1-\eta) &= +(1-\eta)^{n+1}\left(\tfrac{\theta_r}{\theta_r - \bar{T}}\right)\left|\tfrac{\partial \bar{u}}{\partial \eta}\right|^{n-1}\tfrac{\partial^2 \bar{u}}{\partial \eta^2} \\ &+(1-\eta)^n\left[\tfrac{1}{1-\ln\left(\frac{1-\eta}{2}\right)} - 1\right]\left(\tfrac{\theta_r}{\theta_r - \bar{T}}\right)\left|\tfrac{\partial \bar{u}}{\partial \eta}\right|^{n-1}\tfrac{\partial \bar{u}}{\partial \eta} \\ &+(n-1)(1-\eta)^n\left(\tfrac{\theta_r}{\theta_r - \bar{T}}\right)\left|\tfrac{\partial \bar{u}}{\partial \eta}\right|^{n-2}\tfrac{\partial \bar{u}}{\partial \eta}\left[(1-\eta)\tfrac{\partial}{\partial \eta}\left|\tfrac{\partial \bar{u}}{\partial \eta}\right| - \left|\tfrac{\partial \bar{u}}{\partial \eta}\right|\right] \\ &+(1-\eta)^{n+1}\tfrac{\theta_r}{\left(\theta_r - \bar{T}\right)^2}\left|\tfrac{\partial \bar{u}}{\partial \eta}\right|^{n-1}\tfrac{\partial \bar{u}}{\partial \eta} + Ri\bar{T}, \end{aligned} \tag{20}$$

$$\begin{aligned} \tfrac{\partial \bar{T}}{\partial \bar{t}} + \bar{u}\tfrac{\partial \bar{T}}{\partial \xi}(1-\xi) + \bar{v}\tfrac{\partial \bar{T}}{\partial \eta}(1-\eta) &= \tfrac{1}{\mathrm{Pr}}(1-\eta)\left[\tfrac{1}{1-\ln\left(\frac{1-\eta}{2}\right)} - 1\right]\left(1+\varepsilon\bar{T}\right)\tfrac{\partial \bar{T}}{\partial \eta} \\ &+\tfrac{1}{\mathrm{Pr}}\left(1+\varepsilon\bar{T}\right)(1-\eta)^2\tfrac{\partial^2 \bar{T}}{\partial \eta^2} + \tfrac{1}{\mathrm{Pr}}\varepsilon(1-\eta)^2\left(\tfrac{\partial \bar{T}}{\partial \eta}\right)^2, \end{aligned} \tag{21}$$

with the corresponding initial and boundary conditions:

$$\bar{u}(\xi, -1, \bar{t}) = 0, \quad \bar{v}(\xi, -1, \bar{t}) = 0, \quad \bar{T}(\xi, -1, \bar{t}) = 1, \tag{22}$$

$$\bar{u}(\xi, 1, \bar{t}) = 1, \quad \bar{T}(\xi, 1, \bar{t}) = 0, \tag{23}$$

$$\bar{u}(-1, \eta, \bar{t}) = 1, \quad \bar{T}(-1, \eta, \bar{t}) = 0, \tag{24}$$

$$\bar{u}(\xi, \eta, 0) = \bar{u}_0, \quad \bar{T}(\xi, \eta, 0) = \bar{T}_0. \tag{25}$$

3. Numerical solution

In this section we consider the numerical scheme to solve the system of Eqs.(19)-(25). The space and time discretizations are given by the Chebyshev spectral method [8] and third order Runge-Kutta method [5], respectively.

3.1. Chebyshev polynomials. We now recall the basic properties of the weighted orthogonal Chebyshev polynomials [8], which will be used in this paper.

Let T_k be the k-th degree Chebyshev polynomial defined for $x \in [-1, 1]$ as:

$$T_k(x) = \cos(k \arccos x), \qquad k = 0, 1, 2, \cdots. \tag{26}$$

We list the properties that will be used:

$$(i) \quad (T_k, T_j) = \int \frac{1}{\sqrt{1-x^2}} T_k(x) T_j(x) dx = \begin{cases} 0 & k \neq j \\ \pi & k = j = 0 \\ \frac{\pi}{2} & k = j \neq 0 \end{cases}, \tag{27}$$

$$(ii) \quad T_k(\pm 1) = (\pm 1)^k, \tag{28}$$

$$(iii) \quad T_k'(x) = 2k \sum_{\substack{l=0 \\ l+k odd}}^{k-1} \frac{1}{c_l} T_l(x), \quad T_k''(x) = \sum_{\substack{l=0 \\ l+k even}}^{k-2} \frac{1}{c_l} k\left(k^2 - l^2\right) T_l(x), \tag{29}$$

where $c_0 = 2$ and $c_l = 1$ for $l \geq 1$.

3.2. The Chebyshev collocation scheme. For the momentum conservation equation (20) and energy conservation equation (21), we choose the collocation method, which can deal with strongly nonlinear problems easily. For simplicity, we first consider Euler forward time discretization.

First, at time level k, we seek solutions $\bar{u}_{N1,N2}$, $\bar{T}_{N1,N2} \in Q_{N1,N2}$, where $Q_{N1,N2} = \left\{ P : P = \sum_{m=0}^{N1} \sum_{n=0}^{N2} a_{mn} \xi^m \eta^n \right\}$, with N_1, N_2 being the numbers of grid points in the ξ, η directions, respectively. Then we have:

$$\bar{u}_{N1,N2}\left(\xi, \eta, t^k\right) = \sum_{m=0}^{N1} \sum_{n=0}^{N2} \bar{u}_{N1,N2}\left(\xi_m, \eta_n, t^k\right) g_m(\xi) f_n(\eta), \tag{30}$$

$$\bar{T}_{N1,N2}\left(\xi, \eta, t^k\right) = \sum_{m=0}^{N1} \sum_{n=0}^{N2} \bar{T}_{N1,N2}\left(\xi_m, \eta_n, t^k\right) g_m(\xi) f_n(\eta), \tag{31}$$

where $g_m(\xi)$ and $f_n(\eta)$ are the interpolating Lagrange polynomials based on the Gauss-Lobatto quadrature points (ξ_i, η_j) in two space dimension given by:

$$\xi_i = \cos\frac{\pi i}{N1}, \eta_j = \cos\frac{\pi j}{N2}, \forall i = 0, 1 \cdots N1, j = 0, 1 \cdots N2, \tag{32}$$

and $g_m(\xi)$ and $f_n(\eta)$ have the form:

$$g_m(\xi) = \frac{(-1)^{m+1}\left(1 - \xi^2\right) T_N'(\xi)}{C_m N1^2 (\xi - \xi_m)}, f_n(\eta) = \frac{(-1)^{n+1}\left(1 - \eta^2\right) T_N'(\eta)}{C_n N2^2 (\eta - \eta_n)}. \tag{33}$$

By using the Lagrange interpolation, $\bar{u}_{m,n}^k = \bar{u}_{N1,N2}\left(\xi_m, \eta_n, t^k\right)$ is the numerical approximation at the grid point (ξ_m, η_n) at time $t = t^k = k\Delta t$ with Δt being the time step. The solutions are found by requiring the residuals to vanish at the interior collocation points and the grid points on the boundary $\xi = 1$. For simplicity, if we consider the numerical approximation at time level k, the corresponding index k will be omitted. The scheme is:

$$\begin{aligned}
&\frac{\bar{u}_{N1,N2}^{k+1} - \bar{u}_{N1,N2}}{\Delta t} + u_{N1,N2} \frac{\partial \bar{u}_{N1,N2}}{\partial \xi}(1 - \xi) + v_{N1,N2} \frac{\partial \bar{u}_{N1,N2}}{\partial \eta}(1 - \eta) \\
&\quad - (1 - \eta)^{n+1} \left(\frac{\theta_r}{\theta_r - \bar{T}_{N1,N2}}\right) \left|\frac{\partial \bar{u}_{N1,N2}}{\partial \eta}\right|^{n-1} \frac{\partial^2 \bar{u}_{N1,N2}}{\partial \eta^2} \\
&\quad - (1 - \eta)^n \left[\frac{1}{1 - \ln\left(\frac{1-\eta}{2}\right)} - 1\right] \left(\frac{\theta_r}{\theta_r - \bar{T}_{N1,N2}}\right) \left|\frac{\partial \bar{u}_{N1,N2}}{\partial \eta}\right|^{n-1} \frac{\partial \bar{u}_{N1,N2}}{\partial \eta} \\
&-(n-1)(1 - \eta)^n \left(\frac{\theta_r}{\theta_r - \bar{T}_{N1,N2}}\right) \left|\frac{\partial \bar{u}_{N1,N2}}{\partial \eta}\right|^{n-2} \frac{\partial \bar{u}_{N1,N2}}{\partial \eta} \left[(1 - \eta) \frac{\partial}{\partial \eta} \left|\frac{\partial \bar{u}_{N1,N2}}{\partial \eta}\right| - \left|\frac{\partial \bar{u}_{N1,N2}}{\partial \eta}\right|\right] \\
&\quad + (1 - \eta)^{n+1} \frac{\theta_r}{\left(\theta_r - \bar{T}_{N1,N2}\right)^2} \left|\frac{\partial \bar{u}_{N1,N2}}{\partial \eta}\right|^{n-1} \frac{\partial \bar{u}_{N1,N2}}{\partial \eta} - Ri \bar{T}_{N1,N2} = 0,
\end{aligned} \tag{34}$$

$$\begin{array}{c} \frac{\bar{T}^{k+1}_{N1,N2}-\bar{T}_{N1,N2}}{\Delta t}+\bar{u}_{N1,N2}\frac{\partial \bar{T}_{N1,N2}}{\partial \xi}\left(1-\xi\right)+\bar{v}_{N1,N2}\frac{\partial \bar{T}_{N1,N2}}{\partial \eta}\left(1-\eta\right) \\ -\frac{1}{\mathrm{Pr}}\left(1-\eta\right)\left[\frac{1}{1-\ln\left(\frac{1-\eta}{2}\right)}-1\right]\left(1+\varepsilon\bar{T}_{N1,N2}\right)\frac{\partial \bar{T}_{N1,N2}}{\partial \eta} \\ -\frac{1}{\mathrm{Pr}}\left(1+\varepsilon\bar{T}_{N1,N2}\right)\left(1-\eta\right)^{2}\frac{\partial^{2}\bar{T}_{N1,N2}}{\partial \eta^{2}}-\frac{1}{\mathrm{Pr}}\varepsilon\left(1-\eta\right)^{2}\left(\frac{\partial \bar{T}_{N1,N2}}{\partial \eta}\right)^{2}=0, \end{array} \tag{35}$$

for all $\xi=\xi_m, \eta=\eta_n$ with $0\leq m\leq N1-1, 1\leq n\leq N2-1$. To enforce the boundary conditions (22-24), we explicitly require the numerical solution to take the boundary value. For example, for equation (25), we enforce:

$$\bar{u}_{N1,N2}\left(\xi_i,-1,\bar{t}\right)=0, \bar{T}_{N1,N2}\left(\xi_i,-1,\bar{t}\right)=1, \forall i=1,2,\cdots N1. \tag{36}$$

3.3. Chebyshev Galerkin scheme. Now we consider the discretization of the continuum equation (19), in which we would like to use $\bar{u}$ to solve for $\bar{v}$. Notice the fact that, for each fixed ξ, we need only to solve an ODE about $\bar{v}$, therefore we use one dimensional Chebyshev Galerkin method, and choose the basis:

$$\varphi_n\left(\eta\right)=T_n\left(-\eta\right)-1. \tag{37}$$

By (28), such basis satisfies the boundary conditions (22) and clearly $\varphi_0\left(\eta\right)=0$. For each ξ, we seek solutions $\bar{v}_{N1}\left(\eta\right)\in B_{N1}$ such that:

$$\bar{v}_{N1}\left(\eta\right)=\sum_{n=1}^{N1}a_n\varphi_n\left(x\right)=\sum_{n=1}^{N1}a_n\left(T_n\left(-\eta\right)-1\right). \tag{38}$$

To construct the numerical scheme, we want the residual:

$$R_{N1}\left(\eta\right)=\frac{\partial \bar{v}_{N1}}{\partial \eta}\left(1-\eta\right)+\frac{\bar{v}_{N1}}{1-\ln\left(\frac{1-\eta}{2}\right)}+\frac{\partial \bar{u}}{\partial \xi}\left(1-\xi\right) \tag{39}$$

to be orthogonal to $\varphi_n\left(\eta\right)$ in $L^2_w[-1,1]$:

$$\frac{2}{\pi}\int_{-1}^{1}R_{N1}\left(\eta\right)\varphi_k\left(\eta\right)\frac{1}{\sqrt{1-\eta^2}}dx=0, \forall k\in\left[1,2\ldots N1\right]. \tag{40}$$

Here $L^2_w[-1,1]$ is the weighted L^2 space on $[-1,1]$ with the weight function $1/\sqrt{1-\eta^2}$. Notice that for each fixed ξ_m,$\left(1-\xi_m\right)\partial\bar{u}/\partial\xi$ is given. This procedure yields the Chebyshev Galerkin scheme:

$$\begin{array}{c} \int_{-1}^{1}\left(1-\eta\right)\sum\limits_{n=1}^{N1}a_n\varphi_n'\left(\eta\right)\varphi_k\left(\eta\right)\frac{1}{\sqrt{1-\eta^2}}d\eta \\ +\int_{-1}^{1}\frac{1}{1-\ln\left(\frac{1-\eta}{2}\right)}\sum\limits_{n=1}^{N1}a_n\varphi_n\left(\eta\right)\varphi_k\left(\eta\right)\frac{1}{\sqrt{1-\eta^2}}d\eta \\ +\int_{-1}^{1}\frac{\partial\bar{u}}{\partial\xi}\left(1-\xi_m\right)\varphi_k\left(\eta\right)\frac{1}{\sqrt{1-\eta^2}}d\eta=0. \end{array} \tag{41}$$

3.4. Algorithm procedure. We make a summary of the algorithm flowchart. First we consider the initial discretization, and take:

$$\bar{u}^0_{i,j}=\bar{u}_0\left(\xi_i,\eta_j\right), \bar{T}^0_{i,j}=\bar{T}_0\left(\xi_i,\eta_j\right). \tag{42}$$

And then we solve the initial value of vertical velocity $\bar{v}^0$ by applying the Chebyshev Galerkin scheme (41) to the continuum equation (19).

Now suppose we have the numerical approximations at time level k, as $\bar{u}^k, \bar{T}^k$, we use (34)-(35) to obtain $\bar{u}^{k+1}$ and $\bar{T}^{k+1}$, and then use (41) to solve $\bar{v}^{k+1}$.

Finally, to seek the steady state, we compute the L^∞-norm of the velocity difference in the time steps, and we use the following criterion to stop the computation:

$$\left\| \bar{u}^{k+1}_{N1,N2} - \bar{u}^{k}_{N1,N2} \right\|_{L^\infty} \leq 10^{-8}. \tag{43}$$

Besides, we also use FFT to provide a crucial speedup for our calculations, more details can be found in [8].

3.5. High order time discretization scheme. The discretizations above are based on Euler forward time discretization. However, we can also apply the SSP third order Runge-Kutta scheme [5] to improve time accuracy.

For the semi discrete scheme:

$$u_t = L\left(u, t\right), \tag{44}$$

where $L(u,t)$ is a spatial discretization operator, the SSP third order Runge-Kutta scheme is given as:

$$\begin{array}{c} u^{(1)} = u^n + \Delta t L\left(u^n, t^n\right), \\ u^{(2)} = \frac{3}{4}u^n + \frac{1}{4}u^{(1)} + \frac{1}{4}\Delta t L\left(u^{(1)}, t^n + \Delta t\right), \\ u^{n+1} = \frac{1}{3}u^n + \frac{2}{3}u^{(2)} + \frac{2}{3}\Delta t L\left(u^{(2)}, t^n + \frac{1}{2}\Delta t\right). \end{array} \tag{45}$$

In the following numerical experiments we use the SSP third order Runge-Kutta method (45) for the time discretization.

4. Accuracy test and grid testing

In this paper, we use the method of manufactured solutions to test the order of accuracy. First we select appropriate manufactured solutions as following:

$$\bar{u} = e^{\sin(\eta+\xi)}(1+t), \bar{v} = (1 - e^{\sin(\eta+1)})(1+t), \bar{T} = e^{\cos(\eta+\xi)}(1+t). \tag{46}$$

Then we obtain the analytical source term:

$$\frac{\partial \bar{u}}{\partial \xi}\left(1-\xi\right) + \frac{\partial \bar{v}}{\partial \eta}\left(1-\eta\right) + \frac{\bar{v}}{1 - \ln\left(\frac{1-\eta}{2}\right)} = f_1\left(\xi, \eta\right), \tag{47}$$

$$\begin{array}{c} \frac{\partial \bar{u}}{\partial t} + \bar{u}\frac{\partial \bar{u}}{\partial \xi}\left(1-\xi\right) + \bar{v}\frac{\partial \bar{u}}{\partial \eta}\left(1-\eta\right) - \left(1-\eta\right)^n \left[\frac{1}{1-\ln\left(\frac{1-\eta}{2}\right)} - 1\right] \left(\frac{\theta_r}{\theta_r - \bar{T}}\right) \left|\frac{\partial \bar{u}}{\partial \eta}\right|^{n-1} \frac{\partial \bar{u}}{\partial \eta} \\ -\left(n-1\right)\left(1-\eta\right)^n \left(\frac{\theta_r}{\theta_r - \bar{T}}\right) \left|\frac{\partial \bar{u}}{\partial \eta}\right|^{n-2} \frac{\partial \bar{u}}{\partial \eta} \left[\left(1-\eta\right) \frac{\partial}{\partial \eta}\left|\frac{\partial \bar{u}}{\partial \eta}\right| - \left|\frac{\partial \bar{u}}{\partial \eta}\right|\right] \\ -\left(1-\eta\right)^{n+1} \left(\frac{\theta_r}{\theta_r - \bar{T}}\right) \left|\frac{\partial \bar{u}}{\partial \eta}\right|^{n-1} \frac{\partial^2 \bar{u}}{\partial \eta^2} + \left(1-\eta\right)^{n+1} \frac{\theta_r}{\left(\theta_r - \bar{T}\right)^2} \left|\frac{\partial \bar{u}}{\partial \eta}\right|^{n-1} \frac{\partial \bar{u}}{\partial \eta} - Ri\bar{T} = f_2\left(\xi, \eta\right), \end{array} \tag{48}$$

$$\begin{array}{c} \frac{\partial \bar{T}}{\partial t} + \bar{u}\frac{\partial \bar{T}}{\partial \xi}\left(1-\xi\right) + \bar{v}\frac{\partial \bar{T}}{\partial \eta}\left(1-\eta\right) - \frac{1}{\mathrm{Pr}}\left(1-\eta\right)\left[\frac{1}{1-\ln\left(\frac{1-\eta}{2}\right)} - 1\right]\left(1 + \varepsilon\bar{T}\right)\frac{\partial \bar{T}}{\partial \eta} \\ -\frac{1}{\mathrm{Pr}}\left(1 + \varepsilon\bar{T}\right)\left(1-\eta\right)^2 \frac{\partial^2 \bar{T}}{\partial \eta^2} - \frac{1}{\mathrm{Pr}}\varepsilon\left(1-\eta\right)^2 \left(\frac{\partial \bar{T}}{\partial \eta}\right)^2 = f_3\left(\xi, \eta\right) \end{array} \tag{49}$$

with the corresponding initial and boundary conditions. We solve the modified governing equations with these specific source terms on multiple meshes, and then we compute the L^∞-norm for different mesh levels at $t = 0.5$ as shown in Table 1. It is shown that the numerical results achieve spectral convergence in the L^∞-norm until round-off error for double-precision is reached.

Also, for the original dimensionless equations (19)-(25) with

$$\bar{u}_0\left(\xi_i, \eta_j\right) = \frac{\xi_i + 1}{2}, \bar{T}_0\left(\xi_i, \eta_j\right) = \frac{-\xi_i + 1}{2}, \tag{50}$$

TABLE 1. L^∞-norm of the errors between the obtained numerical velocity/temperature solutions and the exact solutions of Eqs. (47)- (49).

GRID	$\bar{u}$		$\bar{v}$		$\bar{T}$	
	ERROR	ORDER	ERROR	ORDER	ERROR	ORDER
4×4	1.49×10^{-3}	–	6.84×10^{-2}	–	2.56×10^{-2}	–
8×8	1.10×10^{-5}	7.08	3.08×10^{-4}	6.64	2.68×10^{-4}	6.58
16×16	4.90×10^{-11}	17.78	3.28×10^{-9}	17.67	1.35×10^{-9}	17.60
32×32	1.37×10^{-10}	–	7.43×10^{-9}	–	1.04×10^{-10}	–

an extensive mesh testing procedure was conducted to guarantee a grid independent solution for code validation, which is shown in Figures 1 and 2. It is found that the results of the calculation change little with a refined (32×32) grid and a coarser (16×16) grid.

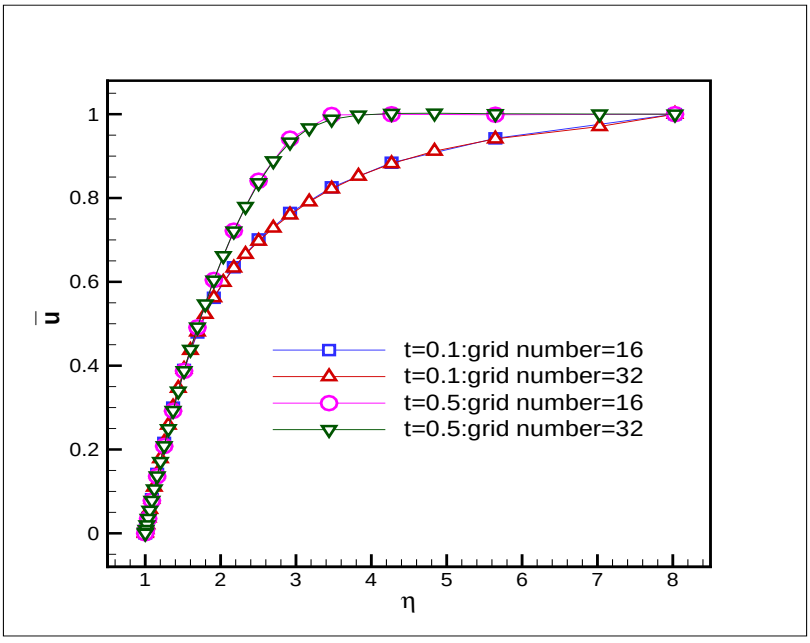

FIGURE 1. Dimensionless velocity profiles for different meshes at $\bar{x} = 0.25$.

5. Results and discussion

In this section, we are going to discuss the physical insights and make a summary. To calculate the velocity and temperature profiles, we solve Eqs. (19) - (21). The

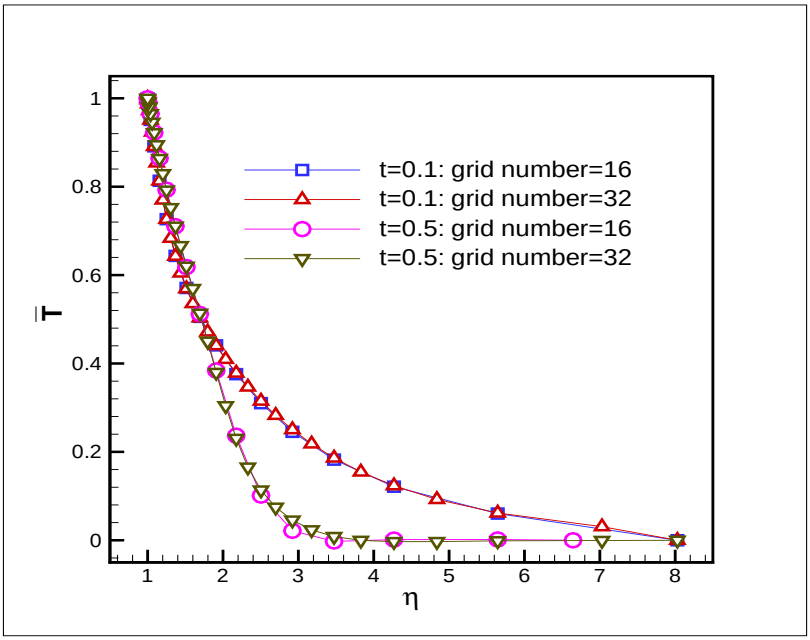

FIGURE 2. Dimensionless temperature profiles for different meshes at $\bar{x} = 0.25$.

initial and boundary conditions are given in (22)-(25) with (50). Then we map the numerical solution back to the $\bar{x}, \bar{r}$ coordinates, see (18) for the mapping. In order to observe the physical insight of the mixed convection boundary layer flow and heat transfer problem, the effects of emerging parameters on the dimensionless velocity profiles and temperature profiles are illustrated graphically in this section.

Figures 3 and 4 show the velocity and temperature distributions of the fields when the steady state has been reached at $t = 1.15$, see section 3.4. The velocity is increasing gradually toward the infinite boundary, while the temperature shows the opposite tendency.

The velocity and temperature profiles with different values of the power law index n are plotted in Figures 5 and 6. As we know, for the case $n = 1$, the fluid is Newtonian, while $n < 1$ and $n > 1$ correspond to pseudo-plastic fluid and dilatant fluid, respectively. It is revealed that the larger the power index n, the smaller the velocity and the thicker the boundary layer. As for the influence on the temperature profile, increasing n results in the growth of the temperature and thermal boundary layer thickness. However, comparing with the velocity profiles, the temperature profiles are less influenced by the power law index.

Figure 7 represents the effects of θ_r, the indicator of the variation of fluid viscosity with temperature, on velocity and temperature distributions, respectively. It is noticed that with an increase in $|\theta_r|$, there is an increase in the momentum boundary layer thickness. This is because, for a given fluid with fixed γ^*, larger $|\theta_r|$ implies smaller temperature difference between the cylinder and the fluid. It is also clear that the velocity changes markedly with smaller $|\theta_r|$, in view of the fact that the higher temperature difference has more significant effect on the fluid viscosity. We add that $\mu(T)$equals to μ_∞, which corresponds to the constant viscosity case when $|\theta_r|$ tends to infinity, for neglecting the effects of variable viscosity on the flow.

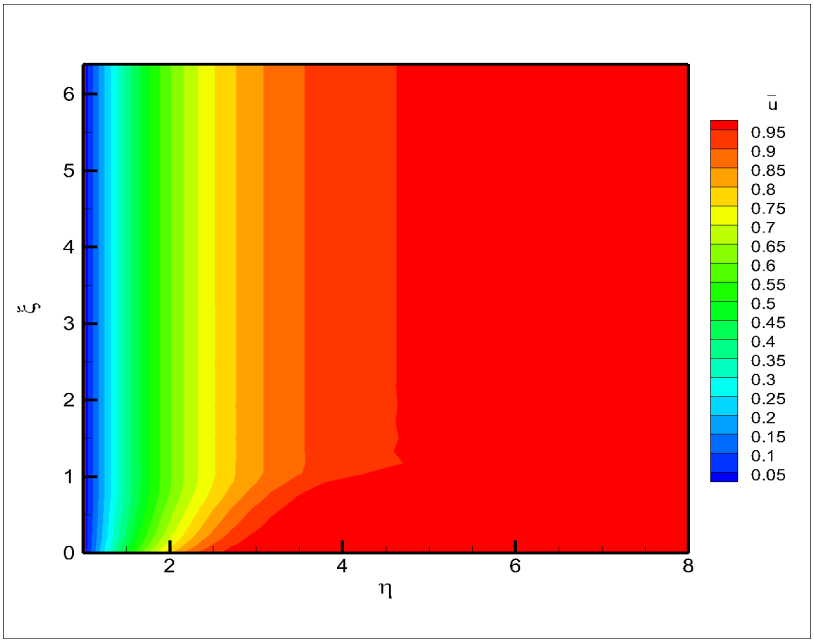

FIGURE 3. Dimensionless velocity field of the steady boundary layer flow when $\bar{t} = 1.15$.

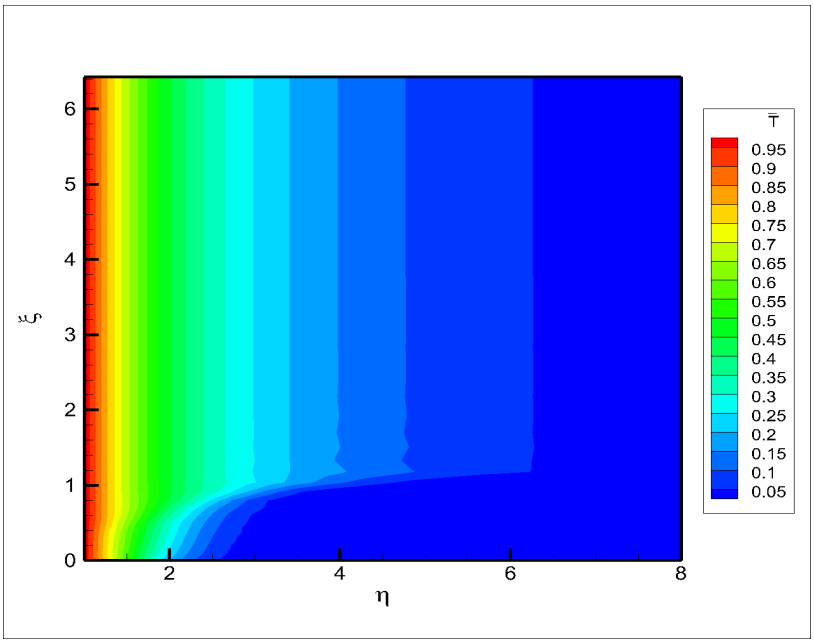

FIGURE 4. Dimensionless temperature field of the steady boundary layer flow when $\bar{t} = 1.15$.

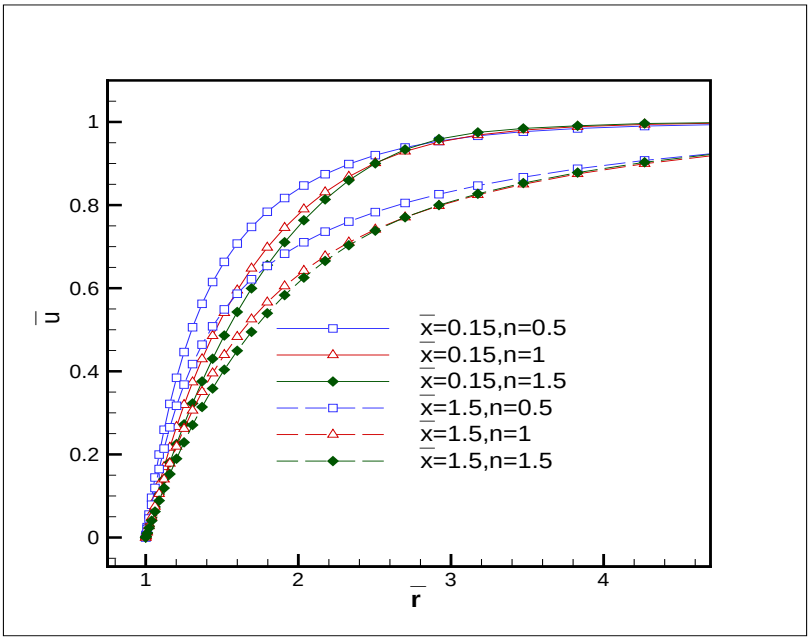

FIGURE 5. Dimensionless velocity profiles for different power law index at $Ri = 0.5, \mathrm{Pr} = 7, \varepsilon = 0.5, \theta_r = -2, \bar{t} = 0.5$.

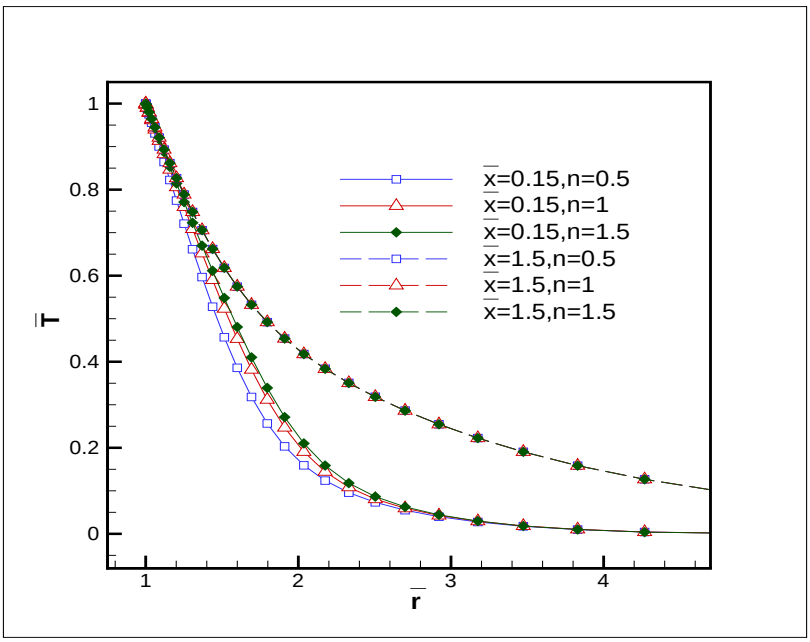

FIGURE 6. Dimensionless temperature profiles for different power law index at $Ri = 0.5, \mathrm{Pr} = 7, \varepsilon = 0.5, \theta_r = -2, \bar{t} = 0.5$.

Moreover, in Figures 8 and 9, we can see that the variable viscosity parameter does not significantly influence the temperature profile, it is similar to the variable thermal conductivity parameter on the velocity profiles.

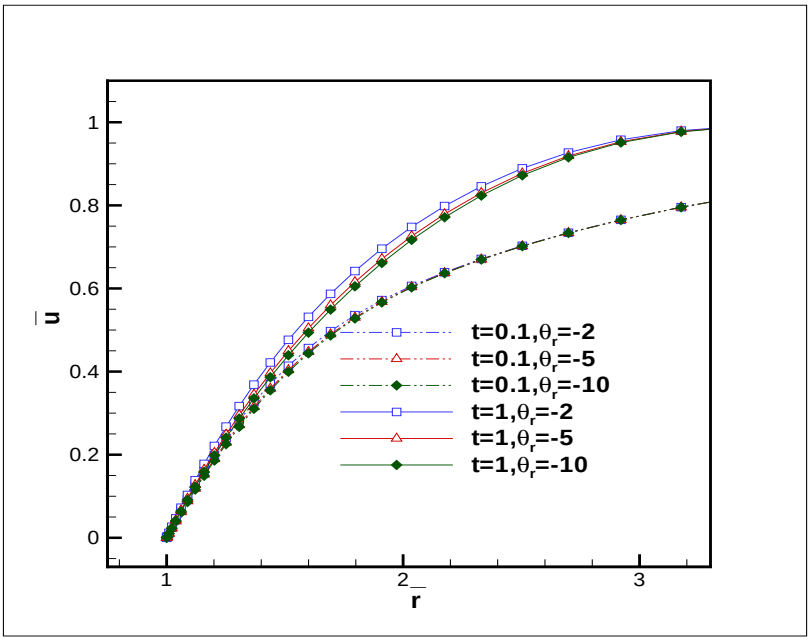

FIGURE 7. Dimensionless velocity profiles for different viscosity parameter at $n = 1.5, Ri = 0.5, \mathrm{Pr} = 7, \varepsilon = 0.5, \bar{x} = 0.25$.

Figure 10 elucidates the variations of temperature profiles with variable thermal conductivity parameter ε. Results show that the dimensionless temperature increases with the increase of ε. Physically, the temperature is found to be low for the constant conductivity of the fluid when $\varepsilon = 0$ compared to the variable case when $\varepsilon > 0$. On the other hand, the thermal boundary becomes thicker in the presence of variable thermal conductivity parameter.

Figures 11 and 12 describe the derived dimensionless velocity and temperature profiles when $n = 1.5, \mathrm{Pr} = 7, \theta_r = -2, \varepsilon = 0.5, \bar{t} = 0.5, \bar{x} = 0.25$ for various values of the Richardson number Ri, which is a measurement of the buoyancy and represents the importance of free convection relative to the forced convection. It is revealed that the velocity increases and the temperature decreases with increasing Ri. Hence the velocity and thermal boundary layer thickness are significantly thinner. The observable phenomenon is attributed to the fact that increasing in Ri gives rise to an increase in the temperature difference between the cylinder and fluid, since a greater Ri indicates a greater buoyancy effect, which leads to an enhancement of the convection and an increase in the surface heat transfer rate. Besides, it shows the overshoot in the velocity profiles near the surface for fluids for higher Ri.

6. Conclusions

In this work we endeavor to investigate unsteady axisymmetric mixed convection heat transfer of power law fluid over a cylinder, and then the temperature dependent

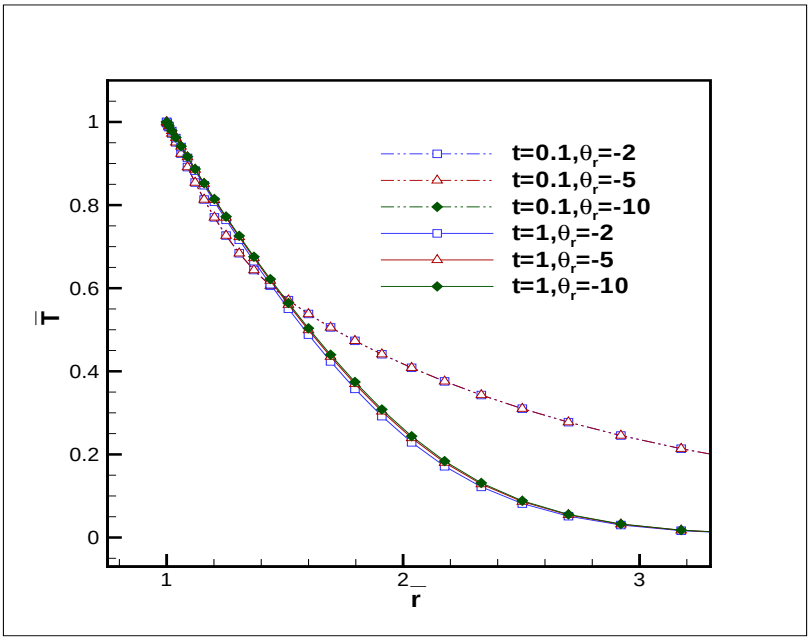

FIGURE 8. Dimensionless temperature profiles for different viscosity parameter at $n = 1.5, Ri = 0.5, \mathrm{Pr} = 7, \varepsilon = 0.5, \bar{x} = 0.25$.

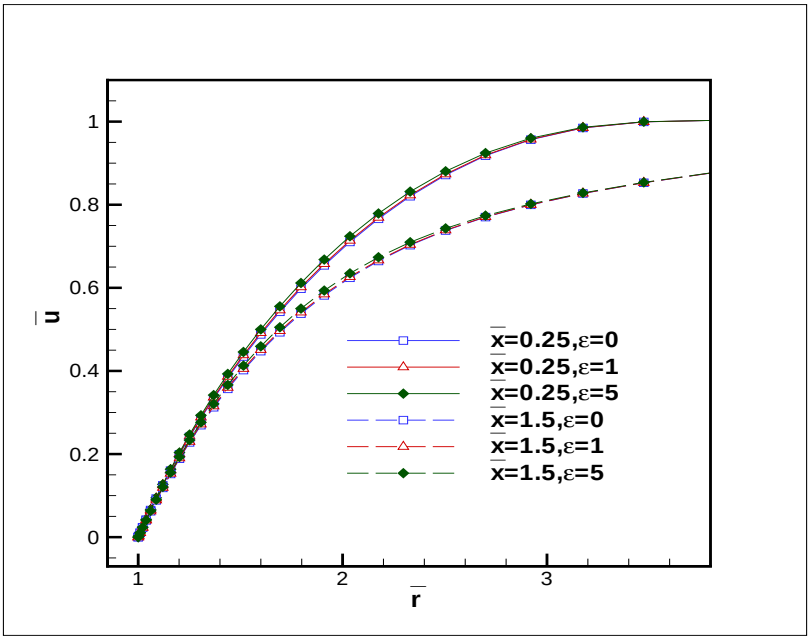

FIGURE 9. Dimensionless velocity profiles for different thermal conductivity parameter at $n = 1.5, Ri = 0.5, \mathrm{Pr} = 7, \theta_r = -2, \bar{t} = 0.5$.

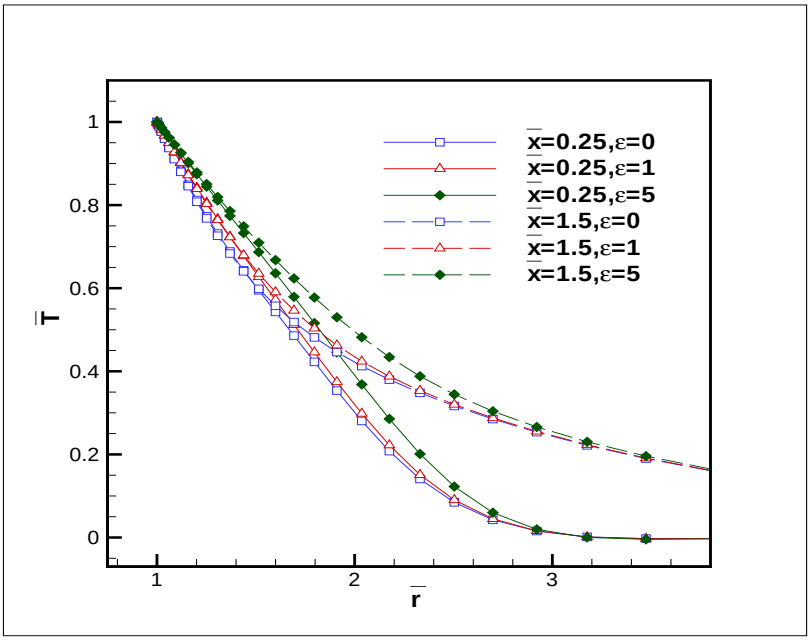

FIGURE 10. Dimensionless temperature profiles for different thermal conductivity parameter at $n = 1.5, Ri = 0.5, \mathrm{Pr} = 7, \theta_r = -2, \bar{t} = 0.5$.

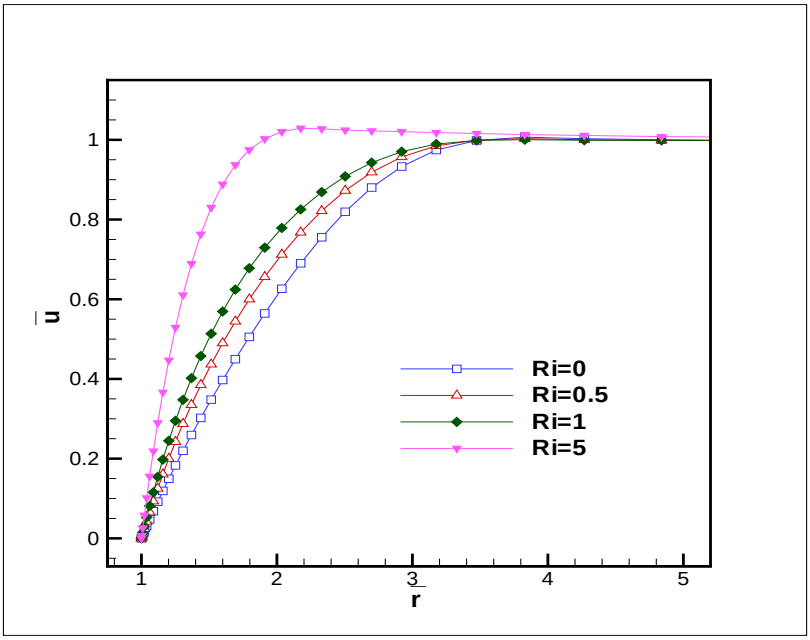

FIGURE 11. Dimensionless velocity profiles for different buoyancy parameters at $n = 1.5, \mathrm{Pr} = 7, \theta_r = -2, \varepsilon = 0.5, t = 0.5, \xi = 0.25$.

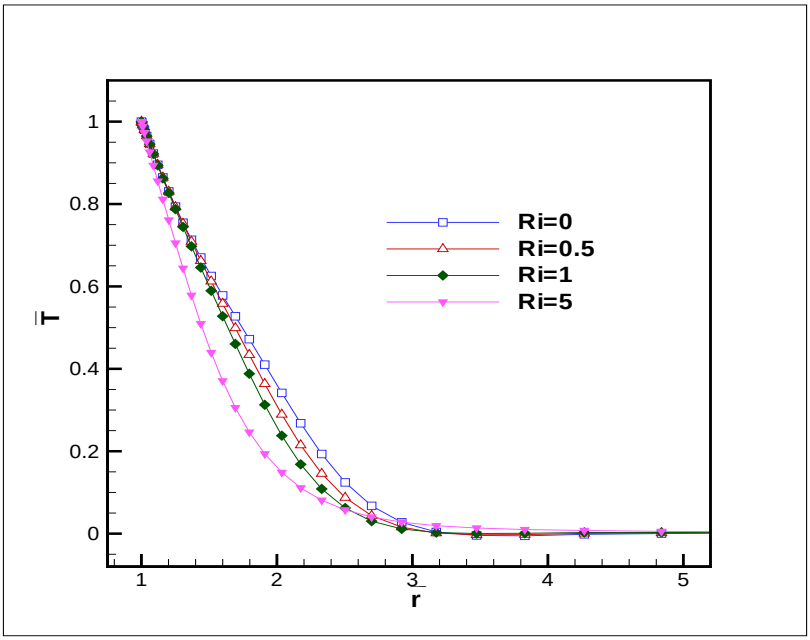

FIGURE 12. Dimensionless temperature profiles for different buoyancy parameters at $n = 1.5, \mathrm{Pr} = 7, \theta_r = -2, \varepsilon = 0.5, \bar{t} = 0.5, \bar{x} = 0.25$.

fluid properties are further studied. From the discussion above, we can arrive at the following conclusions:

(a) Numerical solutions from initial unsteady flow to the final steady flow are obtained by Chebyshev spectral method and SSP third order Runge-Kutta method, and a high order spectral accuracy is observed.

(b) An increase in the power law index n and variable viscosity parameter $|\theta_r|$ decreases the dimensionless velocity and increases momentum boundary layer thickness. However, the Richardson number Ri yields the opposite trend on the velocity profiles. The dimensionless temperature and thermal boundary layer thickness increase as the value of power law index n and thermal conductivity parameter ε increase, while they decrease when the Richardson number Ri increases.

(c) Meanwhile, variable fluid properties result in a visible change of flow and heat transfer characteristics of the power law fluid, hence it is worth mentioning that more investigations might be required in the future to search for variable fluid properties model on non-Newtonian power law fluid.

References

[1] R.P. Bharti, P. Sivakumar and R.P. Chhabra, Forced convection heat transfer from an elliptical cylinder to power-law fluids, Int. J. Heat Mass Transfer, 51 (2008) 1838-1853.

[2] M.N. Bui and T. Cebci, Combined free and forced convection on vertical slender cylinders, ASME J. Heat Transfer, 107 (1985) 476-478.

[3] A. Chandra and R.P. Chhabra, Mixed convection from a heated semi-circular cylinder to power-law fluids in the steady flow regime, Int. J. Heat Mass Transfer, 55 (2012) 214-234.

[4] T.S. Chen and A. Mucoglu, Buoyancy effects on forced convection along a vertical cylinder, ASME J. Heat Transfer, 97 (1975) 198-203.

[5] S. Gottlieb, C.-W. Shu and E. Tadmor, Strong stability-preserving high-order time discretization methods, SIAM Rev., 43 (2001) 89-112.

[6] T. Grosan and I. Pop, Axisymmetric mixed convection boundary layer flow past a vertical cylinder in a nanofluid, Int. J. Heat Mass Transfer, 54 (2011) 3139-3145.
[7] H. Herwig and G. Wickern, The effect of variable fluid properties on laminar boundary layer flow, Warme-und-stoffubertragung, 20 (1986) 47-57.
[8] J.S. Hesthaven, S. Gottlieb and D. Gottlieb, Spectral Methods for Time-Dependent Problems, Cambridge University Press, 2007.
[9] A. Kaya, Effects of buoyancy and conjugate heat transfer on non-Darcy mixed convection about a vertical slender hollow cylinder embedded in a porous medium with high porosity, Int. J. Heat Mass Transfer, 54 (2011) 818-825.
[10] M. Kumari and G. Nath, Mixed convection boundary layer flow over a thin vertical cylinder with localized injection/suction and cooling/heating, Int. J. Heat Mass Transfer, 47 (2004) 969-976.
[11] F.C. Lai and F.A. Kulacki, The effect of variable fluid viscosity on convective heat transfer along vertical surface in a saturated porous medium, Int. J. Heat Mass Transfer, 33 (1990) 1028-1031.
[12] S.L. Lee, T.S. Chen and EF Armaly, Mixed convection along a vertical cylinders and needles with uniform surface heat flux, ASME J. Heat Transfer, 109 (1987) 711-716.
[13] A. Mucoglu and T.S. Chen, Buoyancy effects on forced convection along a vertical cylinder with uniform heat flux, ASME J. Heat Transfer, 98 (1976) 52-55.
[14] S. Mukhopadhyay, Mixed convection boundary layer flow along a stretching cylinder in porous medium, J. Petrol. Sci. Eng., 96-97 (2012) 73-78.
[15] T.G. Myers and J. Low, Modelling the solidification of a power-law fluid flowing through a narrow pipe, Int. J. Thermal Sci., 70 (2013) 127-131.
[16] P.M. Patil, S. Roy and I. Pop, Unsteady effects on mixed convection boundary layer flow from a permeable slender cylinder due to non-linearly power law stretching, Comput. Fluids, 56 (2012) 17-23.
[17] V.K. Patnana, R.P. Bharti and R.P. Chhabra, Two-dimensional unsteady forced convection heat transfer in power-law fluids from a cylinder, Int. J. Heat Mass Transfer, 53 (2010) 4152-4167.
[18] K.V. Prasad, K. Vajravelu and P.S. Datti, Mixed convection heat transfer over a non-linear stretching surface with variable fluid properties, Int. J. Non-Linear Mech., 45 (2010) 320-330.
[19] M.M. Rahman and I.A . Eltayeb, Convective slip flow of rarefied fluids over a wedge with thermal jump and variable transport properties, Int. J. Thermal Sci., 50 (2011) 468-479.
[20] A.M. Rashad, A.J. Chamkha and M. Modather, Mixed convection boundary-layer flow past a horizontal circular cylinder embedded in a porous medium filled with a nanofluid under convective boundary condition, Comput. Fluids, 86 (2013) 380-388.
[21] P.J. Singh, S. Roy and I. Pop, Unsteady mixed convection from a rotating vertical slender cylinder in an axial flow, Int. J. Heat Mass Transfer, 51 (2008) 1423-1430.
[22] A.H. Srinivasa and A.T. Eswara, Unsteady free convection flow and heat transfer from an isothermal truncated cone with variable viscosity, Int. J. Heat Mass Transfer, 57 (2013) 411-420.
[23] K. Vajravelu, K.V. Prasad and C.O. Ng, Unsteady convective boundary layer flow of a viscous fluid at a vertical surface with variable fluid properties, Nonlinear Analysis: RWA, 14 (2013) 455-464.
[24] T.Y. Wang and C. Kleinstruver, General analysis of steady mixed convection heat transfer on vertical slender cylinders, ASME J. Heat Transfer, 111 (1989) 393-398.
[25] Y. Wang and G.A. Chukwu, Application of unsteady couette flow of non-Newtonian power-law fluids in concentric annular wellbore, J. Petrol. Sci. Eng., 17 (1997) 229-235.
[26] L.J. Yang, Q.F. Fu, Y.Y. Qu, B. Gu and M.Z. Zhang, Breakup of a power-law liquid sheet formed by an impinging jet injector, Int. J. Multiphase Flow, 39 (2012) 37-44.

1 School of Mechanical Engineering, University of Science and Technology Beijing, Beijing 100083, China
E-mail: jiajianiu@live.cn

2 School of Mathematics and Physics, University of Science and Technology Beijing, Beijing 100083, China
E-mail: liancunzheng@ustb.edu.cn

3 Department of Mathematical Sciences, Michigan Technological University, Houghton, MI 49931, USA
E-mail: yyang7@mtu.edu

4 Division of Applied Mathematics, Brown University, Providence, RI 02912, USA
E-mail: shu@dam.brown.edu